# A Reaction-diffusion Algorithm for Segmentation of Confocal Laser Scanning Microscope Images

Hiroto Shoji

*Kyoto Prefectural University of Medicine, Sakyo-ku, Kyoto, Kyoto 606-0823, Japan*
*E-mail address: shoji@koto.kpu-m.ac.jp*

(Received October 9, 2016; Accepted November 25, 2016)

The images obtained using a confocal laser scanning microscope (CLSM) alone cannot detect three-dimensional (3D) structures, for example of the endothelial cells that compose blood vessels, and require segmentation for 3D interpretation. Here, we investigated the segmentation of hepatic sinusiodal veins, which form periodic 3D networks. We propose a new approach for image segmentation based on the Turing reaction-diffusion (RD) model. We performed segmentation of CLSM images of sinusoidal endothelial cells using the proposed RD algorithm. Moreover, we discuss potential applications of this algorithm.
**Key words:** Turing Pattern, Reaction-diffusion, Segmentation

## 1. Introduction

Although diffusion processes generally generate uniform distributions of substances, Alan Turing [1] presented the scenario that a spatially periodic pattern is stable in a coupled reaction system with diffusion, if the diffusion coefficients and reaction terms satisfy certain conditions. The pattern induced by the scenario is now called the Turing pattern. Many periodic patterns generated by chemical reactions and biological processes have been examined and explained by the Turing scenario.

Many researchers have investigated utilizing reaction-diffusion (RD) models to perform image processing. Admatzky *et al.* [2] and Ebihara *et al.* [3] proposed algorithms for the segmentation of 2D images utilizing RD models. Using this method, no preprocessing for noise removal, which often affects the accuracy of information extraction, is required.

Although many researchers think that an understanding of 2D periodic patterns is sufficient to explore 3D patterns, we have identified new structures in 3D patterns that cannot be extrapolated from the corresponding 2D structures [4, 5]. Most of these structures are network periodic ones. Therefore, these 3D network structures should be considered as native 3D structures.

Immunostained cells, such as the endothelial cells that compose blood vessels or the cell membranes of hexagonally arranged cells have been studied using CLSM images [6]. However, CLSM images alone cannot detect the full 3D structures. For segmentation of the 3D structures from pixel data obtained by CLSM observation, we propose a new approach based on the Turing RD models. In this forum, we report that we have investigated the periodic network structures of hepatic sinusoidal veins, as an example of CLSM images, using the proposing RD algorithm.



doi:10.5047/forma.2016.005

## 2. Formalism

We considered the following types of RD models:

$$\frac{\partial u(\vec{x},t)}{\partial t} = D_u \delta \nabla^2 u(\vec{x},t) + f(u(\vec{x},t), v(\vec{x},t)) + \epsilon U(\vec{x}), \tag{1}$$

$$\frac{\partial v(\vec{x},t)}{\partial t} = D_v \delta \nabla^2 v(\vec{x},t) + g(u(\vec{x},t), v(\vec{x},t)). \tag{2}$$

where $D_u$, $D_v$, and $\epsilon$ are positive constants. The variable $u(\vec{x},t)$ and $v(\vec{x},t)$ are the local concentrations of two substances. $U(\vec{x})$ denotes the distribution of the pattern obtained by CLSM observation. $\delta$ is the control parameter for space-scaling of the patterns obtained by CLSM observation.

Here, we employ the following reaction terms:

$$f(u(\vec{x},t), v(\vec{x},t)) = u(\vec{x},t) - u(\vec{x},t)^3 - v(\vec{x},t) \text{ and}$$
$$g(u(\vec{x},t), v(\vec{x},t)) = \gamma(u(\vec{x},t) - \alpha v(\vec{x},t) - \beta), \tag{3}$$

where $\alpha$, $\beta$, and $\gamma$ are positive constants [7, 8] selected to satisfy the following conditions in the case of $\epsilon = 0$. The only one equilibrium solution $(\bar{u}, \bar{v})$ given by $\bar{u} - \bar{u}^3 - \bar{v} = 0$ and $\bar{u} - \alpha\bar{v} - \beta = 0$ is stable without diffusion terms, and $(\bar{u}, \bar{v})$ is unstable with respect to fluctuations of a finite wavelength, which are so-called Turing condition [9].

As explained in Murray's textbook [9], static periodic patterns are self-organized when $\epsilon = 0$. When $\epsilon > 0$, the self-organized patterns are entrained to the distribution of $U(\vec{x})$, as shown in Figs. 1(a)–(c). Pixel data contain local differences in fluorescence intensity and inevitable noise. Considering these situations, a distribution of $U(\vec{x})$ was prepared, as shown in Fig. 1(a). Figures 1(a)–(c) show the time evolution. The amplitude of $u(\vec{x},t)$ and local periodicities of $u(\vec{x},t)$ and $U(\vec{x})$ became almost identical throughout.

To incorporate and extend these features of RD models into 3D space, we constructed an RD algorithm for segmentation of CLSM images, as follows. We first scaled the

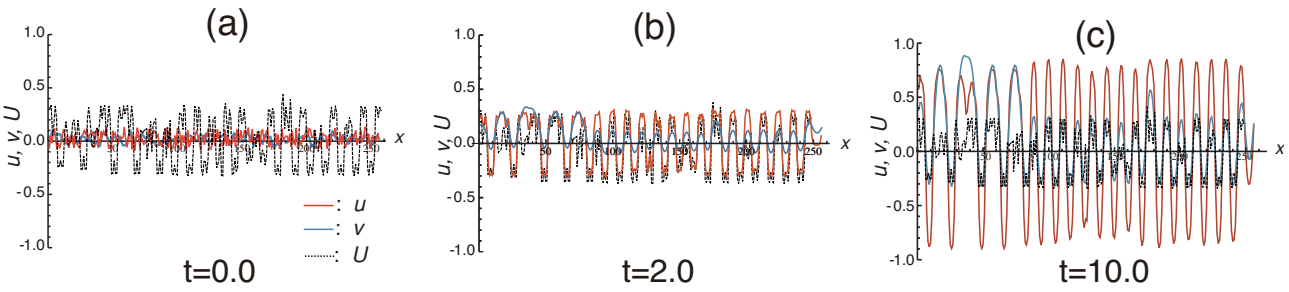


Fig. 1. Formation of spatial patterns obtained from Eqs. (1), (2), and (3) for (a) $t = 0.0$, (b) $t = 2.0$, and (c) $t = 10.0$. The thick red line, the thick blue line, and the dotted black line indicate $u(\vec{x}, t)$, $v(\vec{x}, t)$, and $U(\vec{x})$, respectively.

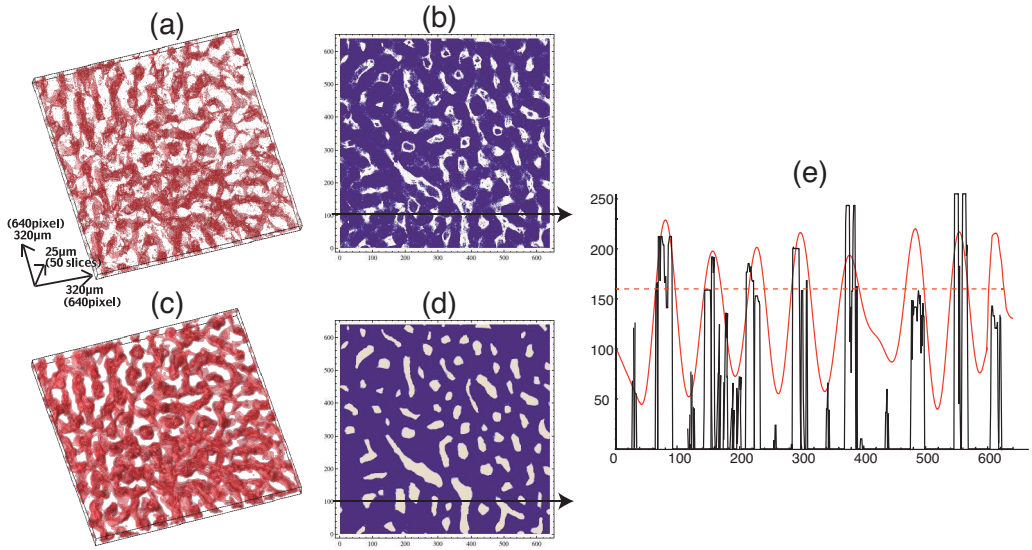


Fig. 2. The 3D reconstructed confocal images of liver sections from rats (a), (b), and their 3D segmentation images obtained using the algorithm proposed here (c), (d). (a) and (c) indicate the 3D patterns of the sinusoidal network (red tubes), and (b) and (d) show the slices at the middle position of the z-axis from (a) and (c), where the white area indicates positions inside the vein. (e) shows the spatial variations of the distributions of pixel data (black line) and the scaled distribution (red line) after RD processing of Eqs. (1) and (2) along the black arrow in (b) and (d). The dotted red line indicates the threshold of segmentations in the image processing, where the values above red line were considered to be inside the vein, and the values below red line were considered to be outside the vein or other types of cells.

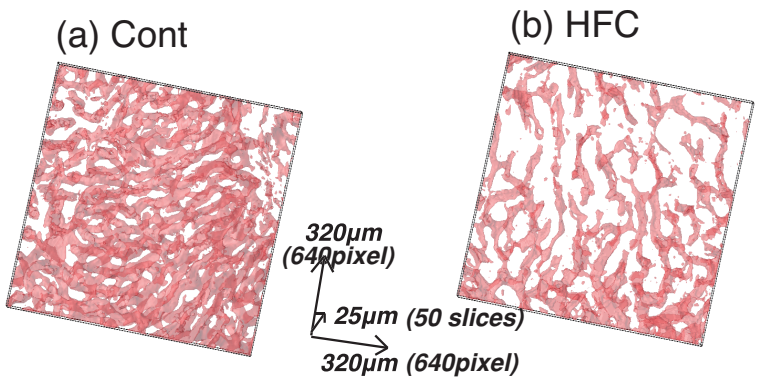


Fig. 3. Examples of 3D segmentation images obtained using the proposed algorithm of Control group (a) and HFC group (b). $\delta^*$ of the control group was $1.00 \pm 0.05$ and that of the HFC group was $1.45 \pm 0.08$. The difference was significant according to the Mann-Whitney $U$-test ($p < 0.01$).

[0,255] scale image of $U(\vec{x})$ into the $[-0.5, 0.5]$ range linearly. Equilibrium values $(\bar{u}, \bar{v})$ for white noise without any spatial correlations were given as the initial distributions of $u(\vec{x}, 0)$ and $v(\vec{x}, 0)$. We performed numerical simulations of Eqs. (1) and (2) with Eq. (3) in three dimensions.

The parameter for space-scaling, $\delta$, was varied in the numerical simulations, whereas the other parameters were fixed. In the case of $\epsilon = 0$, stable periodic patterns with different periodicities are self-organized with changing $\delta$. To examine the most suitable $\delta$ for pixel data obtained by

CLSM, we calculated the correlation between $u$ and $U$ as follows:

$$I(\delta) = \frac{1}{V\sigma_u\sigma_U}\int (u(\vec{x},t)-\bar{u})(U(\vec{x})-\bar{U})d\vec{x} \qquad (4)$$

where $\bar{u}$, $\bar{U}$, $\sigma_u$, and $\sigma_U$ are the mean and the variance of $u$ and $U$. $V$ is the total volume of the region. For each 3D fluorescence image obtained by CLSM, we examined the $\delta^*$ with maximum $I(\delta)$. The final segmentation patterns were obtained using the value of $\delta^*$.

Figure 2 shows an example of 3D segmentation patterns. The 3D images of the raw pixel data are shown in Fig. 2(a), and the slice at the middle position of the z-axis from Fig. 2(a) is shown in Fig. 2(b).

After rescaling the pixel data and introducing $U(\vec{x})$, Eqs. (1), (2) and (3) were calculated in three dimensions. Adjusting the parameter $\delta$, we obtained the 3D segmentation patterns shown in Fig. 2(c) with $\delta^* = 1.05$. The slice at the middle position is shown in Fig. 2(d). The blank portions surrounded by the bright region disappeared.

Moreover, we could automatically remove the inevitable noise in CLSM observation processes during the image processing. In Fig. 2(e), the solid black line indicates the distributions of pixel data obtained by CLSM observation, and the solid red line indicates the scaled distribution of $u(\vec{x},t)$ to [0, 255] after the numerical simulation of Eqs. (1) and (2). Comparing Figs. 2(a)–(d) and Fig. 2(e), we could find that the scaled $u(\vec{x},t)$ in the positions of inevitable noise did not evolve above the threshold for sinusoidal veins, and that the positions of inevitable noise disappeared.

## 3. An Application of this Algorithm: Pattern Recognition in Diseased Rats

Nonalcoholic fatty liver disease (NAFLD), which is related to metabolic syndrome, can cause alteration of the microarchitecture of the liver, because hepatocytes accumulate intracellular fat droplets [10]. We obtained CLSM images of liver sections of rats fed a high-fat/high-cholesterol (HFC) diet for 9 weeks, which causes pathological features similar to those of human patients with NAFLD, and evaluated the 3D patterns using the $\delta^*$ obtained using the RD algorithm [11]. Figure 3 shows the 3D segmentation patterns of sinusoidal networks calculated from fluorescence pixel data using the RD algorithm. The sinusoidal networks of rats in the HFC group, shown in Fig. 3(b), appear tapered or compressed by enlargement of the hepatocytes. Comparison of $\delta^*$ between the HPC and control groups showed a significant difference (data shown in Fig. 3).

## 4. Concluding Remarks

We propose an RD algorithm for segmentation of one type of blood vessels, sinusoid vessels in the liver, from 3D images of sinusoidal endothelial cells obtained by CLSM. The RD model of self-organized distributions was entrained to the distributions of scaled pixel data. Changing the scaling parameter $\delta$ in Eqs. (1) and (2), we were able to capture the periodicity of the sinusoid vessels.

The patterns in living organisms cannot be clearly represented by physical analysis methods such as autocorrelation functions, since the patterns in biological structures often show considerable local variation. However, using the proposed algorithm, $\delta^*$ displayed differences in patterns, even though local variation was present in the patterns. This is one of the advantages of the proposed algorithm.

Another advantage of the algorithm is that it permits elimination of the noise removal algorithm, which is necessary for preprocessing for traditional segmentation methods, and is often sensitive to pattern recognition. In RD model dynamics, using the RD algorithm, noise in the image was automatically removed, enhancing the primary wave patterns, and their amplitude would be almost same among the area.

In this paper, we were able to detect the structure of the sinusoidal network in the liver. This algorithm shows potential for application not only to CLSM images of other organs, but to images obtained using other observation methods. We aim to examine these issues in further detail in future research.

**Acknowledgments.** I would like to thank K. Yamada, National Institute of Technology, Anan College, for fruitful discussions, and K. Hontani, Nagoya Institute of Technology, for helpful comments. This research was supported by JSPS KAKENHI Grant Numbers 26800225 and 15H01125.

## References

[1] Turing, A. M. (1952) The chemical basis of morphogenesis, *Phil. Trans. R. Soc. Lond. B*, **237**, 37–72.
[2] Adamatzky, A., Costello, B. D. L. and Asai, T. (2005) *Reaction Diffusion Computers*, Elsevier, Amsterdam.
[3] Ebihara, M., Mahara, H., Sakurai, T., Nomura, A. and Miike, H. (2003) Segmentation and edge detection of noisy image and low contrast image based on a reaction-diffusion model, *Journal of the Institute of Image Electronics Engineers of Japan*, **32**, 378–385.
[4] Shoji, H., Yamada, K. and Ohta, T. (2007) Interconnected turing patterns in three dimensions, *Phys. Rev.*, **E72**, 065202 (R).
[5] Shoji, H., Yamada, K., Ueyama, D. and Ohta, T. (2007) Turing patterns in three dimensions, *Phys. Rev.*, **E75**, 046212.
[6] Albert, B., Johnson, A., Lewis, J., Raff. M., Roberts, K. and Walter, P. (2014) *Molecular Biology of the Cell*, Garland Science.
[7] FitzHugh, R. (1961) Impulses and physiological states in theoretical models of nerve membrane, *Biophys. J.*, **1**, 445–466.
[8] Nagumo, J., Arimoto, S. and Yoshikawa, Y. (1962) An active pulse transmission line simulating nerve axon, *Proc. IRE*, **50**, 2061–2071.
[9] Murray J. D. (1989) *Mathematical Biology*, Springer, New York.
[10] Sheila, S. and Dooley, J. (2002) *Diseases of the Liver and Biliary System*, Wiley-Blackwell.
[11] Shoji, H. and Yamada, K. (2016) A reaction-diffusion algorithm for segmentation of three-dimensional sinusoidal networks in rats fed a high-fat and high-coresterol diet: New insights and evaluation (submitted).